

Effective embedded-atom potential for metallic adsorbates on crystalline surfaces

This content has been downloaded from IOPscience. Please scroll down to see the full text.

2014 Modelling Simul. Mater. Sci. Eng. 22 035015

(<http://iopscience.iop.org/0965-0393/22/3/035015>)

View [the table of contents for this issue](#), or go to the [journal homepage](#) for more

Download details:

IP Address: 193.49.32.117

This content was downloaded on 01/07/2015 at 12:07

Please note that [terms and conditions apply](#).

Effective embedded-atom potential for metallic adsorbates on crystalline surfaces

G D Förster, Y Magnin, F Rabilloud and F Calvo

Institut Lumière Matière, UMR 5306 Université Claude Bernard Lyon 1 - CNRS,
Université de Lyon, 10 rue Ada Byron, F 69622 Villeurbanne Cedex, France

E-mail: florent.calvo@univ-lyon1.fr

Received 2 December 2013, revised 12 February 2014

Accepted for publication 14 February 2014

Published 21 March 2014

Abstract

Based on the embedded-atom method (EAM), an analytical effective potential is developed to model the interaction of a metallic adsorbate on a perfect crystalline substrate, which is also metallic. The many-body character of the original EAM potential is preserved in the adsorbate energy and in the alteration of the substrate energy due to the presence of the adsorbate. A mean-field-type version neglecting corrugation of the substrate is first derived based on rigorous integration of individual monolayers, followed by an approximate form for the perturbation of the substrate energy. Lateral corrugation is subsequently included by additional phenomenological terms respecting the symmetry of the substrate, again preserving the many-body nature of the original potential. The effective model contains four parameters to describe uncorrugated substrates and eight extra parameters to describe every order of the Fourier lateral expansion. These parameters were fitted to reproduce the adsorption energy of a sample of random configurations of realistic 2D and 3D clusters deposited on the (1 1 1) fcc surface, for metals for which popular EAM models have been parametrized. As a simple application, the local relaxation of pre-formed icosahedral or truncated octahedral clusters soft-landed and exposing (1 1 1) faces in epitaxy to the substrate has been simulated at 0 and 300 K. The deformation of small clusters to wet the substrate is correctly captured by the effective model. This agreement with the exact potential suggests that the present model should be useful for treating metallic environments in large-scale surface studies, notably in structural optimization or as a template for more general models parametrized from *ab initio* data.

Keywords: embedded-atom model, metallic adsorbates, crystalline substrate, effective potential

(Some figures may appear in colour only in the online journal)

1. Introduction

Despite continuous advances in electronic structure methods, the atomistic modeling of materials still largely relies on analytical potentials, which allow much larger systems to be treated over long time scales. One further step in alleviating a major part of the computational cost consists of using implicit models to simplify the description of the environment around the system of interest. Such a simplification is desirable at least when the system and its environment do not exchange particles or share electrons, a problem also found in hybrid schemes of quantum chemistry such as quantum mechanics/molecular mechanics [1] or in the treatment of solvent effects by continuum approximations [2].

An archetypal situation where the environment can often be clearly partitioned is that of an adsorbate deposited on a crystalline substrate. At the lowest level of chemical complexity, rare-gas atoms adsorbed on flat surfaces represent the simplest case for which effective potentials integrating the complete environment have been rigorously derived [3]. The popularity of the Steele potential, although associated with the existence of accurate pairwise potentials between rare-gas atoms, has led to various extensions for environments having different geometries, such as nanotubes [4] or cylindrical pores [5]. Ionic adsorbates on dielectric or conducting surfaces can also be treated by additive potentials, with possible complications due to polarization effects that may be addressed using image charges [6]. Metallic adsorbates represent an important category for which the interaction with dielectric substrates is often oversimplified into purely pairwise forces [7]¹. More realistic approaches have been followed, with coordination-dependent contributions representing electron flow more accurately with respect to *ab initio* reference data [8, 9].

Metallic adsorbates on metallic substrates are of considerable importance in surface physics, as in the structure, energetics and wetting of adsorbed clusters [10–22], their thermodynamics [17], their diffusion and dissociation dynamics [10, 12, 23–43] already at the limit of single adatoms [44–54]. These studies are assisted by the availability of structural information provided experimentally by scanning tunneling microscopy or transmission electron microscopy. From the computational perspective, cohesion in metals cannot be accurately modelled by simple pair potentials, because electron delocalization leads to a strong dependence on the local environment of each atom, a feature that is essential in the description of both surfaces and adsorbates. For transition and noble metals, many-body analytic potentials derived from the moments of electronic densities of states in tight-binding theory [55, 56] represent a major advance in the computational study of materials. They have been revived and greatly disseminated by the so-called embedded-atom method (EAM) [57] and its extensions [58, 59], which also include a common framework for bond-order potentials [60].

No effective potential for a metallic substrate that also supports a metallic adsorbate has been proposed so far. The difficulties mostly lie in the non-additive character of the many-body EAM potentials, making the substrate cohesion energy depend non-trivially on the presence of the adsorbate. However, the development of an implicit potential for incorporating those many-body effects into the energetics of an adsorbate would shift most of the computational effort devoted to the substrate to the description of the adsorbate itself, enabling numerical studies on a statistical footing and tasks such as structural optimization. It is the purpose of the present article to show that, at least for a popular type of EAM potential, such an effective model can be obtained for adsorbates on flat crystalline surfaces, at the cost of only a limited number of approximations. The analytical potential we extracted contains a reduced set of

¹ For instance, many simulation studies have relied on the simple Lennard-Jones potential to model the interaction between metal nanoparticles and graphitic substrates.

parameters, and appears accurate for a broad range of situations. Although derived from a specific underlying EAM model, the form obtained for the implicit potential should be useful as a generic template for modeling metallic adsorbates on crystalline substrates.

The article is organized as follows. In the next section, we properly define the problem at hand and introduce the notations. Section 3 presents a first effective potential in the case where the substrate is uncorrugated and treated at the mean-field level. Section 4 extends this model to account for lateral corrugation by means of phenomenological corrections that preserve the required symmetry of the substrate. The application to realistic metals is presented and discussed in section 5, where effective potentials for the (1 1 1) face-centered cubic substrates are trained for all metals parametrized by Cleri and Rosato [61]. In section 6, we present a simple application of the model to the local relaxation of nickel clusters performed in the gas phase and soft-landed on the (1 1 1) nickel substrate. The effective potential correctly reproduces not only the adsorption energies, but also the magnitude of the deformation as the clusters undergo thermal motion at 300 K. Based on these results, we finally give some concluding remarks in section 7.

2. Notations and definitions

We consider an N -atom system with Cartesian coordinates $\mathbf{R} = \{r_i, i = 1, \dots, N\}$. The system is partitioned into the substrate (sub) and the adsorbate (ads). The total binding energy is written according to the following EAM-type potential, also known in the literature as a second-moment approximation (SMA) to the electronic density of states in tight-binding theory [55, 56, 62]:

$$\begin{aligned} V(\mathbf{R}) &= V_{\text{rep}}(\mathbf{R}) + V_{\text{at}}(\mathbf{R}) \\ &= \sum_{i,j \neq i} \varepsilon \exp \left[-p \left(\frac{r_{ij}}{r_0} - 1 \right) \right] - \sum_i \left\{ \sum_{j \neq i} \xi^2 \exp \left[-2q \left(\frac{r_{ij}}{r_0} - 1 \right) \right] \right\}^{1/2} \\ &= \sum_{i,j \neq i} \varepsilon f_{\text{rep}}(r_{ij}) - \sum_i \left\{ \sum_{j \neq i} \xi^2 f_{\text{at}}(r_{ij}) \right\}^{1/2}, \end{aligned} \quad (1)$$

where we have introduced the pairwise repulsive contribution V_{rep} and the many-body attractive contribution V_{at} that involve the exponential functions f_{rep} and f_{at} , which depend on the distance r_{ij} between atoms i and j . The attractive contribution can also be expressed using the embedding function $F = \sqrt{n}$ and the effective electronic density n as

$$\begin{aligned} V_{\text{at}}(\mathbf{R}) &= - \sum_i F(n_i), \\ n_i &= \sum_{i \neq j} \xi^2 f_{\text{at}}(r_{ij}). \end{aligned}$$

In writing equation (1), we have assumed for simplicity that the adsorbate and the substrate are constituted of the same metal. This assumption is mainly for the sake of notations, because different metals could be treated as well, with additional parameters reflecting the interactions between alike and unlike atoms. The exponential forms chosen for f_{rep} and f_{at} will be essential in the following, as they allow most continuous and discrete integrals to be evaluated exactly. Applications of EAM potentials to large-scale materials usually truncate all distance-dependent functions beyond some cut-off designed to alleviate most of the computational cost, which then roughly scales linearly with the number of atoms. In the present work, this approximation is

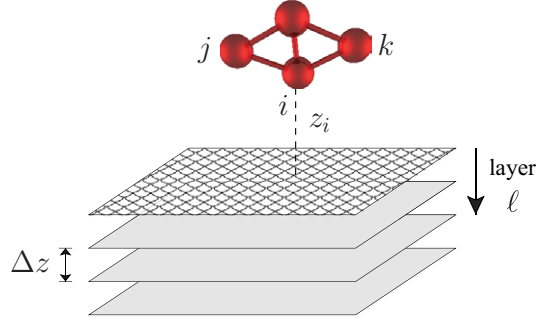


Figure 1. Adsorbate deposited over an infinite series of flat monolayers. The corrugation is only shown for the uppermost layer.

unnecessary and even unwanted, as integrals of exponentially decaying functions are more conveniently evaluated in the entire physical domain.

We initially tried to represent the uncorrugated substrate as a uniform density medium. The effective potential, already at the stage of its pairwise repulsive part, appeared to be incompatible from the exact reference potential at the full atomistic level. This observation led us to follow instead the Steele strategy [3], in which the substrate is represented as an infinite series of monolayers distant by Δz (see figure 1). Surface relaxation, which is ignored at this stage, will subsequently be restored.

Our next objective in this work is to integrate the substrate in equation (1), giving an effective potential V_{eff} that implicitly accounts for the environment of the adsorbate. We have distinguished two levels of approximation for the effective potential, starting the derivation for the laterally averaged (or uncorrugated) potential \bar{V}_{eff} , in which the layers are assumed to be uniform. A complete effective potential with corrugation, V_{eff} , will be proposed next.

3. Uncorrugated model

The first steps of our integration deal with a simplified description of the substrate, assumed not to carry any lateral dependence. This mean-field level of approximation already provides great insight into the effective potential, and will allow the generic form to be extracted.

3.1. Uniform monolayer

The monolayer is assumed to lie at height $z = 0$, with the adsorbate atoms located above ($z_i > 0$). The repulsive potential is additive and can be partitioned into the three contributions

$$\bar{V}_{\text{rep}}(\mathbf{R}) = \bar{V}_{\text{rep}}^{(\text{ads})}(\mathbf{R}) + \bar{V}_{\text{rep}}^{(\text{sub})}(\mathbf{R}) + \bar{V}_{\text{rep}}^{(\text{int})}(\mathbf{R}),$$

where we distinguish the pure adsorbate (ads), the pure substrate (sub) and the adsorbate-substrate interactions (int), respectively. The pure substrate energy $\bar{V}_{\text{rep}}^{(\text{sub})}$ does not depend on the presence of the adsorbate and is not considered further. For integration purposes, the substrate layer is assumed to be uniform with a surface density σ :

$$\bar{V}_{\text{rep}}^{(\text{ads})} = \sum_{i,j \in \text{ads}, i \neq j} \varepsilon f_{\text{rep}}(r_{ij}),$$

$$\bar{V}_{\text{rep}}^{(\text{int})} = 2 \sum_{i \in \text{ads}} \sigma \iint d^2r_j \varepsilon f_{\text{rep}}(r_{ij}),$$

where $\sum_{i \in \text{ads}}$ denotes a sum over adsorbate atoms only. The double integral can be calculated exactly as

$$\bar{V}_{\text{rep}}^{(\text{int})} = \sum_{i \in \text{ads}} 4\pi\sigma \left(\frac{r_0}{p}\right)^2 \left(1 + p\frac{z_i}{r_0}\right) \varepsilon f_{\text{rep}}(z_i).$$

Turning now to the attractive contribution, we notice that it is *not additive*; hence the partition into substrate, adsorbate and interacting components made for the repulsive part is no longer possible. Instead, the adsorbate modifies the energy of the layer as

$$\bar{V}_{\text{at}}(\mathbf{R}) = \bar{V}_{\text{at}}^{(\text{ads})}(\mathbf{R}) + \bar{V}_{\text{at}}^{(\text{sub})}(\mathbf{R}).$$

The adsorbate term $\bar{V}_{\text{at}}^{(\text{ads})}$ can be expressed by integration of the substrate contribution:

$$\begin{aligned} \bar{V}_{\text{at}}^{(\text{ads})} &= - \sum_{i \in \text{ads}} \left\{ \sum_{j \in \text{ads}, j \neq i} \xi^2 f_{\text{at}}(r_{ij}) + \sigma \xi^2 \iint d^2\mathbf{r}_j f_{\text{at}}(r_{ij}) \right\}^{1/2} \\ &= - \sum_{i \in \text{ads}} \left\{ \sum_{j \in \text{ads}, j \neq i} \xi^2 f_{\text{at}}(r_{ij}) + 2\pi\sigma \xi^2 \left(\frac{r_0}{2q}\right)^2 \left(1 + 2q\frac{z_i}{r_0}\right) f_{\text{at}}(z_i) \right\}^{1/2}. \end{aligned}$$

We now have to evaluate the contribution of the adsorbate to the substrate energy. Since the substrate is infinite, its energy diverges and we only need to consider the difference due to the presence of the adsorbate:

$$\begin{aligned} \bar{V}_{\text{at}}^{(\text{sub})} &= -\sigma \iint d^2\mathbf{r}_j \left\{ \xi^2 \sum_{i \in \text{ads}} f_{\text{at}}(r_{ij}) + \sigma \xi^2 \iint d^2\mathbf{r}_i f_{\text{at}}(r_{ij}) \right\}^{1/2} \\ &\quad + \sigma \iint d^2\mathbf{r}_j \left\{ \sigma \xi^2 \iint d^2\mathbf{r}_i f_{\text{at}}(r_{ij}) \right\}^{1/2} \\ &= -\sigma \iint d^2\mathbf{r}_j \frac{V_{\text{ads}}^2}{[V_{\text{ads}}^2 + V_s^2]^{1/2} + V_s}, \end{aligned} \quad (2)$$

where we have used the identity $\sqrt{a} - \sqrt{b} = (a - b)/(\sqrt{a} + \sqrt{b})$ and the notation

$$V_{\text{ads}}^2(\mathbf{r}_j) = \sum_{i \in \text{ads}} \xi^2 f_{\text{at}}(r_{ij}),$$

V_s^2 denoting the (squared) attractive energy of individual atoms of the pure monolayer:

$$V_s^2 = \sigma \xi^2 \iint d^2\mathbf{r}_i f_{\text{at}}(r_i) = 2\pi\sigma \xi^2 \left(\frac{r_0}{2q}\right)^2 e^{2q}.$$

If the adsorbate consists of a single adatom, then $V_{\text{at}}^{(\text{sub})}$ has a closed form as

$$\bar{V}_{\text{at}}^{(\text{sub})} = -2\pi\sigma \int_{z_i}^{\infty} r \, dr \frac{\xi^2 f_{\text{at}}(r)}{[\xi^2 f_{\text{at}}(r) + V_s^2]^{1/2} + V_s} = -2\pi\sigma \xi \mathcal{I}(z_i),$$

where \mathcal{I} is short for

$$\mathcal{I}(z) = \int_z^{\infty} r \, dr \frac{f_{\text{at}}(r)}{[f_{\text{at}}(r) + V_s^2/\xi^2]^{1/2} + V_s/\xi}.$$

This integral can be calculated numerically as a function of z_i (notice that \mathcal{I} does not depend on ξ). A simple approximate form may be preferred to avoid evaluating the integral \mathcal{I} in simulations, and tests indicate that an appropriate expression is

$$\mathcal{I}(z) \simeq (az + b) f_{\text{at}}(z),$$

with a and b two parameters to be fitted. This leads to our final expression for the contribution of the adsorbate to the substrate energy difference in the case of a single adatom:

$$\bar{V}_{\text{at}}^{(\text{sub})} \simeq -2\pi\sigma\xi(a z_i + b) f_{\text{at}}(z_i).$$

If the adsorbate contains more than one atom, the expression for $\bar{V}_{\text{at}}^{(\text{sub})}$ cannot be further integrated without approximation. To do so, we start by realizing that $\bar{V}_{\text{at}}^{(\text{sub})}$ remains exactly additive:

$$\bar{V}_{\text{at}}^{(\text{sub})} = - \sum_{i \in \text{ads}} \sigma \int \int d^2 \mathbf{r}_j \frac{\xi^2 f_{\text{at}}(r_{ij})}{[\sum_{k \in \text{ads}} \xi^2 f_{\text{at}}(r_{jk}) + V_s^2]^{1/2} + V_s},$$

but the sum in the denominator prevents analytical integration. In order to produce a suitable approximation, we note that the effect of the sum $\sum_{k \in \text{ads}}$ in this denominator consists of attenuating the fraction as much as there are atoms neighboring to j . Putting aside the (i, j) contribution $f_{\text{at}}(r_{ij})$ from the sum, the remaining contribution of the other atoms k can be approximated as a coordination correction f_{cor} , in such a way that

$$\begin{aligned} \bar{V}_{\text{at}}^{(\text{sub})} &\simeq - \sum_{i \in \text{ads}} f_{\text{cor}} \sigma \int \int d^2 \mathbf{r}_j \frac{\xi^2 f_{\text{at}}(r_{ij})}{[\xi^2 f_{\text{at}}(r_{ij}) + V_s^2]^{1/2} + V_s} \\ &= - \sum_{i \in \text{ads}} f_{\text{cor}} 2\pi\sigma\xi \mathcal{I}(z_i), \end{aligned} \quad (3)$$

and in which the following empirical expression was found after several attempts to correctly account for the many-body perturbation of the adsorbate on the substrate energy:

$$f_{\text{cor}} = \left\{ A \sum_{k \neq i} \exp \left[-2q \left(\frac{z_k}{r_0} - 1 \right) \right] \times \exp \left[-2q \left(\frac{r_{ik}}{r_0} - 1 \right) \right] + B \right\}^{-1/2}, \quad (4)$$

with A and B being two additional parameters requiring optimization. Equation (3) expressed our main approximation in deriving an effective potential for metallic adsorbates on flat substrates based on SMA many-body potentials. While the parameters a and b only provide convenient replacements for an otherwise time-consuming 1D integral, A and B are related to the correcting factor f_{cor} , which plays an important role in capturing the many-body effects in the way the adsorbate affects the substrate cohesion. Despite this intrinsic difference, and for additional reasons detailed in the next section, those four quantities were treated on the same footing during parametrization on reference data.

3.2. Infinite succession of planes

We now turn to the more realistic problem where the substrate consists of an infinite set of monolayers separated by Δz from one another. In doing so, we assume no surface relaxation or reconstruction of the substrate, which is of course not realistic in general and especially for gold. However, the final potential being adjusted on the truly optimized substrate, the parameters will implicitly carry relaxation effects.

With this assumption, the binding energy can still be partitioned into the repulsive and attractive contributions for the pure adsorbate and substrate. For the repulsive contribution, the result is

$$\bar{V}_{\text{rep}}^{(\text{int})} = \sum_{i \in \text{ads}} 4\pi\sigma\varepsilon \left(\frac{r_0}{p} \right)^2 \left[\sum_{\ell=0}^{\infty} \left(1 + p \frac{z_i + \ell \Delta z}{r_0} \right) f_{\text{rep}}(z_i + \ell \Delta z) \right].$$

Owing to the exponential form of f_{rep} , the infinite series can be calculated exactly as

$$\bar{V}_{\text{rep}}^{(\text{int})} = \sum_{i \in \text{ads}} 4\pi\sigma\varepsilon \left(\frac{r_0}{p}\right)^2 f_{\text{rep}}(z_i) [\alpha_p(1 + pz_i/r_0) + \gamma_p],$$

where we have introduced the two fixed quantities α_p and γ_p as

$$\alpha_p = \frac{1}{1 - \exp(-p\Delta z/r_0)};$$

$$\gamma_p = \frac{p\Delta z}{r_0} \frac{\exp(-p\Delta z/r_0)}{[1 - \exp(-p\Delta z/r_0)]^2}.$$

Concerning now the attractive contribution, the modification of the adsorbate energy due to the multiple layers can similarly be expressed as the infinite sum

$$\bar{V}_{\text{at}}^{(\text{ads})} = - \sum_{i \in \text{ads}} \left\{ \sum_{j \in \text{ads}, j \neq i} \xi^2 f_{\text{at}}(r_{ij}) + 2\pi\sigma \left(\frac{r_0}{2q}\right)^2 \xi^2 \sum_{\ell=0}^{\infty} \left(1 + 2q \frac{z_i + \ell\Delta z}{r_0}\right) f_{\text{at}}(z_i + \ell\Delta z) \right\}^{1/2}$$

$$= - \sum_{i \in \text{ads}} \left\{ \sum_{j \in \text{ads}, j \neq i} \xi^2 f_{\text{at}}(r_{ij}) + 2\pi\sigma \left(\frac{r_0}{2q}\right)^2 \xi^2 f_{\text{at}}(z_i) [\alpha_{2q}(1 + 2qz_i/r_0) + \gamma_{2q}] \right\}^{1/2},$$

where we have used the same notations for α_{2q} and γ_{2q} as for α_p and γ_p (see above).

The substrate energy is also modified for multiple layers, but this perturbation relative to the substrate without adsorbate is additive over the layers

$$\bar{V}_{\text{at}}^{(\text{sub})} = \sum_{\ell=0}^{\infty} \bar{V}_{\text{at}}^{(\text{sub}, \ell)},$$

with $\bar{V}_{\text{at}}^{(\text{sub}, \ell)}$ the energy difference for layer ℓ ,

$$\bar{V}_{\text{at}}^{(\text{sub}, \ell)} = -\sigma \iint d^2\mathbf{r}_j \frac{V_{\text{ads}, \ell}^2}{[V_{\text{ads}, \ell}^2 + V_{s, \ell}^2]^{1/2} + V_{s, \ell}}, \quad (5)$$

where we have extended the notation $V_{\text{ads}, \ell}^2(\mathbf{r}_{j, \ell})$ to describe the squared attractive energy between the adsorbate and layer ℓ of the substrate:

$$V_{\text{ads}, \ell}^2(\mathbf{r}_{j, \ell}) = \sum_{i \in \text{ads}} \xi^2 f_{\text{at}}(r_{ij, \ell}).$$

In equation (5), we have also denoted by $V_{s, \ell}^2$ the squared attractive energy of the entire layer ℓ , per atom of this layer and in absence of the adsorbate. As was the case for V_s^2 , this constant quantity can be evaluated exactly because all series can be summed:

$$V_{s, \ell}^2 = V_s^2 \left\{ 1 + \frac{\exp(-2q\Delta z/r_0)}{1 - \exp(-2q\Delta z/r_0)} [2 - \exp(-2q\ell\Delta z/r_0)] \right.$$

$$\left. + \frac{2q\Delta z}{r_0} \frac{\exp(-2q\Delta z/r_0)}{[1 - \exp(-2q\Delta z/r_0)]^2} [2 - (\ell + 1)\exp(-2q\ell\Delta z/r_0) + \ell \exp(-2q(\ell + 1)\Delta z/r_0)] \right\}.$$

We finally use the same approximation for $\bar{V}_{\text{at}}^{(\text{sub},\ell)}$ as was used for the single layer, introducing a coordination correction $f_{\text{cor}}^{(\ell)}$ (equation (4)):

$$\begin{aligned} V_{\text{at}}^{(\text{sub},\ell)} &\simeq - \sum_{i \in \text{ads}} \sigma f_{\text{cor}}^{(\ell)} \iint d^2 r_j \frac{\xi^2 f_{\text{at}}(r_{ij})}{[\xi^2 f_{\text{at}}(r_{ij}) + V_{s,\ell}^2]^{1/2} + V_{s,\ell}} \\ &= - \sum_{i \in \text{ads}} 2\pi \sigma \xi f_{\text{cor}}^{(\ell)} \mathcal{I}_\ell(z_i + \ell \Delta z) \\ &\simeq - \sum_{i \in \text{ads}} 2\pi \sigma \xi f_{\text{cor}}^{(\ell)} \times (a_\ell(z_i + \ell \Delta z) + b_\ell) f_{\text{at}}(z_i + \ell \Delta z), \end{aligned}$$

where the parameters a_ℓ and b_ℓ must be fitted to reproduce the continuous integral \mathcal{I}_ℓ . In practice, for the examples discussed below, a_ℓ and b_ℓ are found to converge with increasing ℓ already at the fourth layer.

An important additional simplification was made by only considering the contribution $\bar{V}_{\text{at}}^{(\text{sub},0)}$, hereafter simply denoted $\bar{V}_{\text{at}}^{(\text{sub})}$, from the uppermost layer, thus neglecting all deeper layers and accounting implicitly for possible symmetry-preserving surface reconstructions in the reference system. This approximation was found to work satisfactorily, provided that all parameters a , b , A and B are adjusted accordingly to reproduce reference data from the training set.

To summarize, the first effective potential proposed in this work to describe the cohesion of a metallic adsorbate deposited on a flat crystalline but uncorrugated metal surface is written as

$$\begin{aligned} \bar{V}_{\text{eff}}(\mathbf{R}) &= \sum_{i,j \neq i} \varepsilon e^{-p(r_{ij}/r_0-1)} + \sum_i 4\pi \sigma \varepsilon \left(\frac{r_0}{p}\right)^2 [\alpha_p(1 + pz_i/r_0) + \gamma_p] e^{-p(z_i/r_0-1)} \\ &- \sum_i \left\{ \sum_{j \neq i} \xi^2 e^{-2q(r_{ij}/r_0-1)} + 2\pi \sigma \xi^2 \left(\frac{r_0}{2q}\right)^2 [\alpha_{2q}(1 + 2qz_i/r_0) + \gamma_{2q}] e^{-2q(z_i/r_0-1)} \right\}^{1/2} \\ &- \sum_i 2\pi \sigma \xi \left\{ A \sum_{j \neq i} e^{-2q(z_i/r_0-1)} e^{-2q(r_{ij}/r_0-1)} + B \right\}^{-1/2} [(az_i + b)e^{-2q(z_i/r_0-1)}]. \quad (6) \end{aligned}$$

This potential cannot be reduced as a simple sum between the contributions from the adsorbate and substrate alone. The many-body nature of the original SMA potential is reflected by the presence of an additional contribution from the substrate on the adsorbate (third term on the right hand side of equation (6)) and by the entire last term that describes the perturbation of the substrate energy due to the adsorbate. The form above contains only four parameters (a , b , A and B) that must be optimized for any specific situation.

4. Accounting for lateral corrugation

The effective potential of the previous section and its accuracy is probably more relevant for describing moderate- to high-energy problems of collisions on substrates in which the structural details close to the surface are not essential. However, at low temperatures the potential may be of less interest due to the importance of corrugation.

The average potential \bar{V}_{eff} for uncorrugated substrates was derived by a maximum number of exact integrations, assuming uniform densities and flat monolayers. In contrast, we treat corrugation phenomenologically by modifying \bar{V}_{eff} in such a way that the lateral periodicity of the substrate is incorporated by additional dedicated terms.

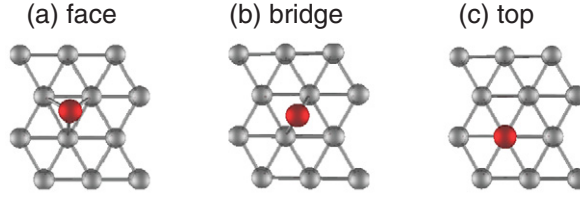


Figure 2. Three lateral positions for the adatoms used to determine the lateral forms and parameters of the corrugation part of the potential (shown here for a single adatom).

Corrugation impacts the effective potential at different places. For the average potential \bar{V}_{eff} we consider an additive corrugation contribution V_{cg} , plus some terms in the many-body components $V_{\text{at}}^{(\text{ads})}$ and $V_{\text{at}}^{(\text{sub})}$. All corrugation terms respect the symmetry of the surface lattice, taking into account only the first terms of the Fourier expansion. For instance, for the additive term V_{cg} , we write

$$V_{\text{cg}}(\mathbf{R}) = \sum_{k=1}^{k_{\text{max}}} \sum_i V_g^{(k)}(z_i) f_k(x_i, y_i),$$

where the functions f_k are the successive orders of the Fourier expansion up to order k_{max} , and $V_g^{(k)}$ represents a correcting potential. An appropriate form for $V_g^{(k)}(z)$ was initially obtained by fitting the difference between the potential of a single deposited atom at the three positions of face, bridge and top (see figure 2), and the average potential as a function of z . The resulting variations could be correctly fitted using a generalized Morse function:

$$V_g^{(k)}(z) = C_k \exp\left[-\mu_k \left(\frac{z}{r_0} - 1\right)\right] - D_k \exp\left[-\nu_k \left(\frac{z}{r_0} - 1\right)\right], \quad (7)$$

with C_k, μ_k, D_k, ν_k four parameters (per Fourier order k) to be determined.

Besides this additive correction, lateral corrections were also applied to the many-body attractive part $\bar{V}_{\text{at}}^{(\text{ads})}$ and to the substrate energy difference $\bar{V}_{\text{at}}^{(\text{sub})}$ as follows:

$$V_{\text{at}}^{(\text{ads})} = - \sum_{i \in \text{ads}} \left\{ \sum_{j \in \text{ads}, j \neq i} \xi^2 f_{\text{at}}(r_{ij}) + 2\pi\sigma\xi^2 \left(\frac{r_0}{2q}\right)^2 [\alpha_{2q}(1 + 2qz_i/r_0) + \gamma_{2q}] f_{\text{at}}(z_i) + \sum_{k=1}^{k_{\text{max}}} V_g^{(\text{ads},k)}(z_i) f_k(x_i, y_i) \right\}^{1/2},$$

$$V_{\text{at}}^{(\text{sub})} = - \sum_{i \in \text{ads}} 2\pi\sigma\xi f_{\text{cor}} \left[\mathcal{I}(z_i) + \sum_{k=1}^{k_{\text{max}}} \mathcal{I}^{(k)}(z_i) f_k(x_i, y_i) \right],$$

where simple exponential functions are used for $V_g^{(\text{ads},k)}$ and \mathcal{I}_k :

$$V_g^{(\text{ads},k)}(z) = W_k^2 \exp\left[-\omega_k \left(\frac{z}{r_0} - 1\right)\right],$$

$$\mathcal{I}^{(k)}(z) = I_k \exp\left[-\rho_k \left(\frac{z}{r_0} - 1\right)\right].$$

Lateral corrugation is thus described by a set of $8k_{\text{max}}$ parameters, namely, $C_k, D_k, \mu_k, \nu_k, W_k, I_k, \omega_k$ and ρ_k , that need to be optimized in order to reproduce the energies of a training set.

To summarize, the fully corrugated effective potential proposed here reads

$$\begin{aligned}
V_{\text{eff}}(\mathbf{R}) = & \sum_{i,j \neq i} \varepsilon e^{-p(r_{ij}/r_0-1)} + \sum_i 4\pi\sigma\varepsilon \left(\frac{r_0}{p}\right)^2 [\alpha_p(1 + pz_i/r_0) + \gamma_p] e^{-p(z_i/r_0-1)} \\
& - \sum_i \left\{ \sum_{j \neq i} \xi^2 e^{-2q(r_{ij}/r_0-1)} + 2\pi\sigma\xi^2 \left(\frac{r_0}{2q}\right)^2 [\alpha_{2q}(1 + 2qz_i/r_0) + \gamma_{2q}] e^{-2q(z_i/r_0-1)} \right. \\
& \left. + \sum_{k=1}^{k_{\max}} W_k e^{-\omega_k(z_i/r_0-1)} f_k(x_i, y_i) \right\}^{1/2} \\
& + \sum_i \sum_{k=1}^{k_{\max}} [C_k e^{-\mu_k(z_i/r_0-1)} - D_k e^{-\nu_k(z_i/r_0-1)}] f_k(x_i, y_i) \\
& - \sum_i 2\pi\sigma\xi \left\{ A \sum_{j \neq i} e^{-2q(z_i/r_0-1)} e^{-2q(r_{ij}/r_0-1)} + B \right\}^{-1/2} \\
& \times \left[(az_i + b) e^{-2q(z_i/r_0-1)} + \sum_{k=1}^{k_{\max}} I_k e^{-\rho_k(z_i/r_0-1)} f_k(x_i, y_i) \right].
\end{aligned}$$

Note that due to the two latter corrections in $V_{\text{at}}^{(\text{ads})}$ and $V_{\text{at}}^{(\text{sub})}$, the laterally averaged effective potential $\langle V_{\text{eff}} \rangle$ is not strictly equivalent to the uncorrugated potential \bar{V}_{eff} of the previous section:

$$\langle V_{\text{eff}} \rangle(z) = \sigma \iint_{\text{unit cell}} V_{\text{eff}}(x, y, z) dx dy \neq \bar{V}_{\text{eff}}(z).$$

Numerical tests indicate, however, that the difference is not very significant, an observation that will be exploited in practice to produce a single set of parameters for both the average and corrugated effective potentials.

5. Application to (1 1 1) fcc surfaces

As a testing ground, the capability of the above effective potentials to represent the exact SMA energy for realistic adsorbates on substrates was investigated for the most compact (1 1 1) fcc surfaces, for which the present frozen substrate is the least questionable, and for the 10 transition and noble metals for which the SMA potential was parametrized by Cleri and Rosato [61]. Although these specific sets of parameters were fitted to reproduce bulk properties only, it should be noted that such potentials perform well for low-dimensional systems including surfaces [63], nanowires [64] and clusters [65].

In the case of the (1 1 1) fcc surface, truncating the lateral Fourier expansion at second order requires the two following basis functions:

$$\begin{aligned}
f_1(x_i, y_i) &= \cos \left[\frac{2\pi}{d} \left(x_i + \frac{y_i}{\sqrt{3}} \right) \right] + \cos \left[\frac{2\pi}{d} \left(x_i - \frac{y_i}{\sqrt{3}} \right) \right] + \cos \left(\frac{4\pi}{d} \frac{y_i}{\sqrt{3}} \right); \\
f_2(x_i, y_i) &= \cos \left[\frac{2\pi}{d} \left(x_i + y_i \sqrt{3} \right) \right] + \cos \left[\frac{2\pi}{d} \left(x_i - y_i \sqrt{3} \right) \right] + \cos \left(\frac{4\pi}{d} x_i \right),
\end{aligned}$$

$d = r_0$ being the lattice constant of the fcc surface.

The corrugated potential derives from the uncorrugated version by the addition of lateral corrections in both the pair energy and the many-body adsorbate energy. For \bar{V}_{eff} , the

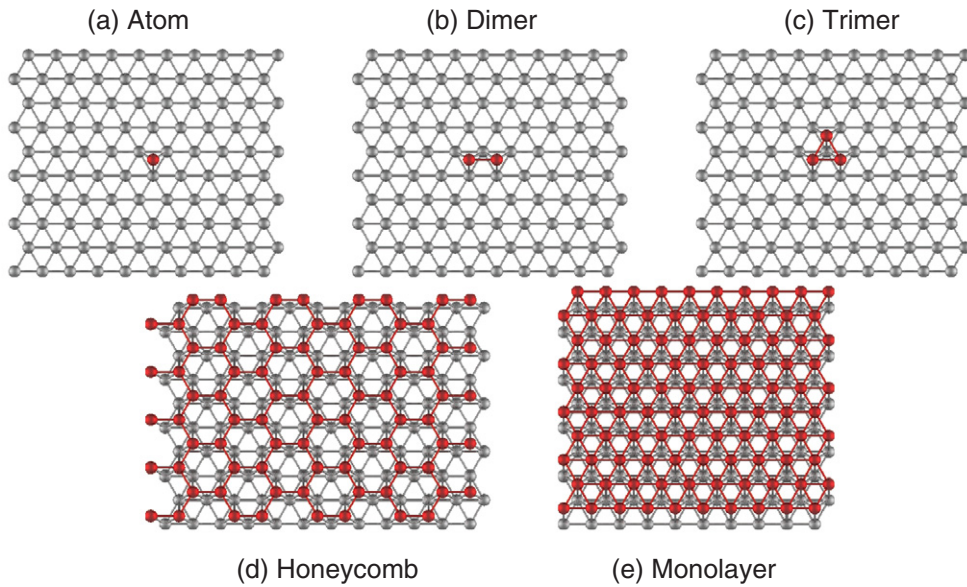


Figure 3. Types of adsorbates on the (1 1 1) fcc surface with high symmetry and fixed coordination. (a) single atom; (b) dimer; (c) trimer; (d) honeycomb; (e) full monolayer.

parameters a_ℓ and b_ℓ employed to represent the integrals \mathcal{I}_ℓ are in principle well defined from the variations of the exact function \mathcal{I}_ℓ . However, by approximating the entire substrate to its uppermost layer, those parameters are best left free in the optimization process, together with the empirical parameters A and B . Additionally, although B should be 1 for single adatoms, improved flexibility was gained by leaving it free during the fitting procedure.

For the corrugated substrate, our phenomenological introduction of extended Morse functions for the two Fourier orders results in eight additional parameters, to which eight more parameters are included to account for the lateral variations in the many-body contributions $V_g^{(\text{ads},k)}$ and $\mathcal{I}^{(k)}$.

We have followed a two-step hierarchical optimization procedure by first evaluating the four parameters a , b , A and B by adjusting the variations of the binding energy of five flat adsorbates as their distance to the surface increases, by standard minimization of a least-square error function χ^2 . Those adsorbates were chosen to be subparts of a (1 1 1) fcc monolayer, differing only in their coordination number C . More precisely, they are depicted in figure 3 and consist of a single adatom ($C = 0$), a dimer ($C = 1$), a trimer ($C = 2$), a honeycomb lattice ($C = 3$) or a full monolayer ($C = 6$). Although not as broad as the range covered by actual 3D nanostructures, the coordination numbers spanned by those adsorbates appear sufficiently widespread for the potential to correctly capture the many-body effects.

For these five adsorbates, reference energy profiles $V_C(z)$ describing the effective interaction with the substrate were obtained by suitable lateral averaging of the exact SMA energy, removing the contributions of the adsorbate and substrate at infinite separation. All calculations assumed periodic boundary conditions along the lateral x and y directions, for both the adsorbates and substrates.

The accuracy of the potential \bar{V}_{eff} so obtained was tested against a series of 300 configurations generated by random geometry perturbations from a flat 7-atom adsorbate and from a 13-atom and a 55-atom icosahedral cluster, depicted in figure 4. The remaining

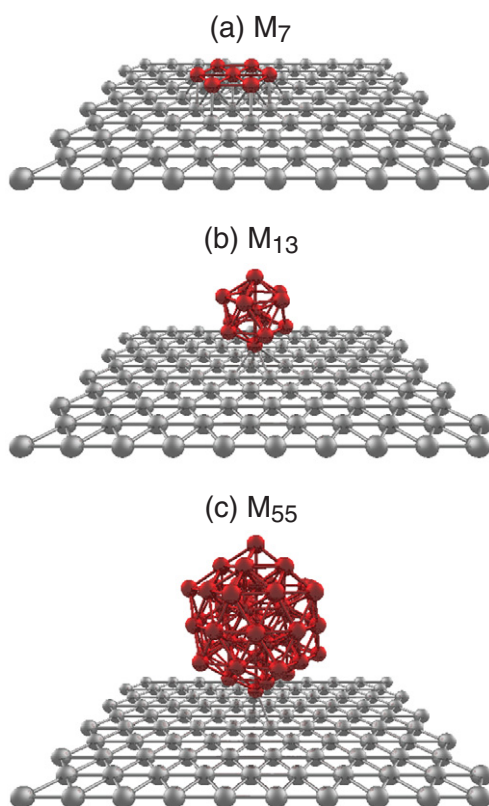


Figure 4. Adsorbates employed to generate random configurations for the training set used to parametrize the lateral components of the effective potential. (a) 7-atom hexagonal island; (b) 13-atom icosahedral cluster; (c) 55-atom icosahedral cluster.

sets of parameters were initially fitted using the same flat adsorbates with fixed height, only considering specific lateral positions on the face, bridge or top sites. This procedure turned out not to be accurate enough to represent the reference energies of the random adsorbates. Fitting the parameters directly against those energies appeared to be a more robust strategy, which we have adopted for all metals.

The final set of parameters obtained for gold are given in table 1, with the parameters for the nine other metals tabulated in the appendix. From a general point of view, the parameters obtained for the second-order Fourier terms are generally much smaller than those at first order, indicating that truncating the lateral expansion at this order is sufficient for those metals, stopping at first order (with 4+8 parameters instead of 4+8+8) already providing a reasonable picture of the adsorbate–substrate interaction.

The energy profiles for the average effective interaction \bar{V}_{eff} between the flat adsorbates of figure 3 and the laterally averaged (1 1 1) fcc substrate are represented in figure 5(a) for the specific case of gold.

This profile illustrates the importance of many-body effects in the adsorption on surfaces: at equilibrium, the binding energy *per atom* is attenuated as the adsorbate size (or coordination number) increases. The effective potential \bar{V}_{eff} accurately reproduces this behavior for the various flat adsorbates considered as our first training set, and the same quality of adjustment

Table 1. List of all parameters of the effective potential for gold metallic adsorbates on the (1 1 1) fcc surface. The original SMA parameters from Cleri and Rosato [61] are also given.

Parameter	Value	Parameter	Value
ε	0.2061 eV	p	10.229
ξ	1.790 eV	q	4.036
r_0	2.8843 Å		
a	3.975×10^{-2} Å	A	6.38×10^{-4}
b	0.021×10^{-2} Å ²	B	38.8×10^{-2}
C_1	36.1×10^{-2} eV	μ_1	10.37
D_1	36.9×10^{-2} eV	ν_1	9.97
C_2	1.179×10^{-3} eV	μ_2	12.14
D_2	1.20×10^{-3} eV	ν_2	3.52
W_1	4.04×10^{-2} eV	ω_1	10.11
I_1	1.059×10^{-3} Å ²	ρ_1	5.11
W_2	7.49×10^{-3} eV	ω_2	4.53
I_2	4.79×10^{-5} Å ²	ρ_2	5.63

is found for the second training set of random clusters adsorbed on the (1 1 1) gold substrate (results not shown).

However, and as previously mentioned, keeping the parameters a , b , A and B fixed and adjusting the remaining 16 parameters for lateral corrugation so that the full effective potential V_{eff} reproduces the exact potential for the face, bridge and top positions generally degrades the agreement for the second training set of random configurations. Fitting the complete set of 20 parameters on this random set significantly improves the quality of the resulting potential, as illustrated in figure 6(b), where the value of V_{eff} is represented against the exact adsorption energy for the 300 random cluster configurations.

The correlation between the exact and effective potentials is very good, with a Pearson regression coefficient R^2 approaching 0.999. It is worth noting that using the four parameters a , b , A and B in the uncorrugated version \bar{V}_{eff} of the potential preserves its accuracy to a very satisfactory extent, as shown in figure 6(a). The even higher correlation ($R^2 = 0.9992$) is consistent with the fewer variables involved in the averaged potential, in which the complex sensitivity to many-body effects is partly washed out by the lateral averaging procedure.

Although an even higher correlation is obtained by specifically fitting the four specific parameters a , b , A and B for \bar{V}_{eff} , the present level of agreement between both effective models and the corresponding reference potentials seems satisfactory for most applications dealing with the structure or dynamical properties.

The effective potentials derived in this paper are thus accurate, and could be easily extended to describe other surface crystallinities with other suitable basis functions $f_k(x, y)$. Of course, the accuracy could be further improved by extending the Fourier expansion to higher order. However, this would probably be undesirable for an optimal computational efficiency, and the fitting procedure for numerous parameters might become a daunting task requiring a larger and non-redundant training set.

Adsorbates made of a different metal could also be studied with the same effective potentials, as long as parameters for the reference SMA model are available. Those situations

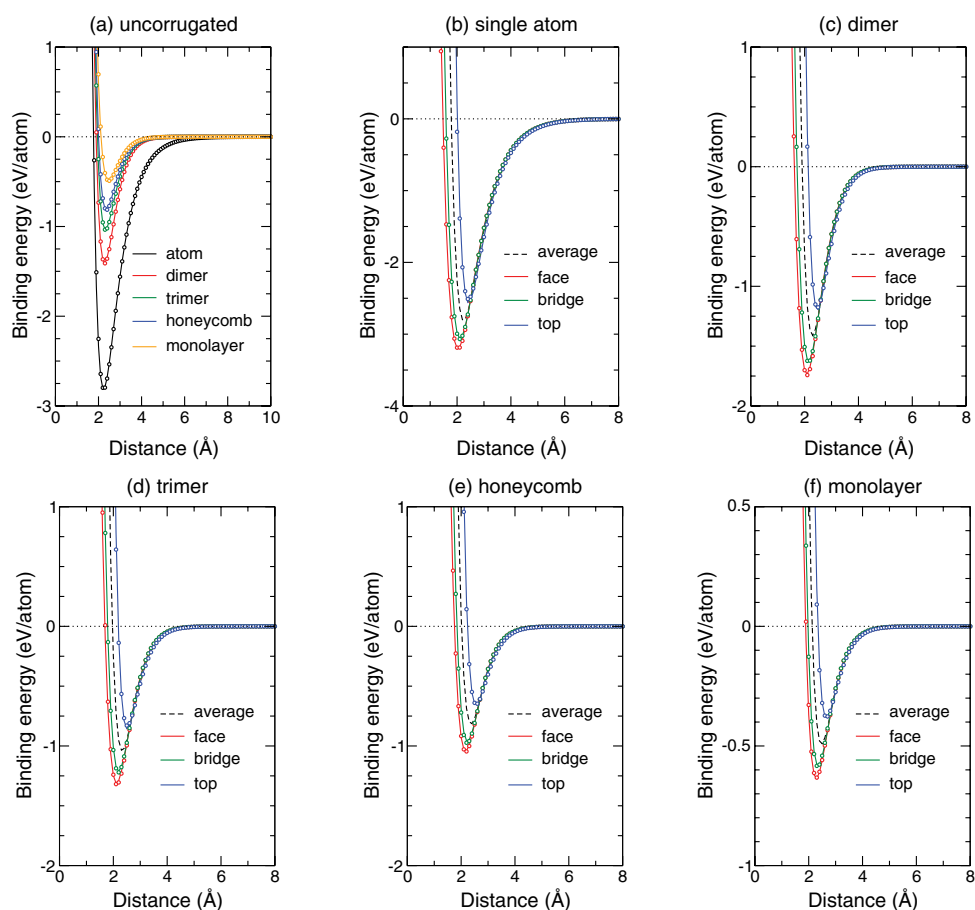


Figure 5. Interaction energy of the five flat adsorbates of gold on the (1 1 1) fcc gold substrate, as a function of their distance to the uppermost layer. (a) Effective potential for the uncorrugated surface; (b)–(f) Full effective potential for a single adatom, a dimer, a trimer, the honeycomb and full layer adsorbed on the substrate at different lateral positions corresponding to the face, bridge and top sites. The dots are the results of the effective potentials, and lines refer to the exact SMA potential. For panels (b)–(f), the dashed lines denote the laterally averaged or uncorrugated potential.

would actually be even more suitable for the present implicit approaches, since dynamical processes at finite temperature such as the diffusion or dissociation of adsorbates on substrates of the same (or less cohesive) metals may involve the displacement of atoms from the uppermost layers [30, 44, 45, 47, 49]. A particularly relevant case would be that of alloyed substrates such as random solutions or metallic glasses, for which structural disorder may be integrated through appropriate weighting functions.

Although based on simple functions, the SMA potentials have a rigorous connection with tight-binding theory [55, 56, 62] and are reasonably accurate for bulk fcc metals as well as low-dimensional systems [63–65]. Better potentials can of course be afforded at the cost of more complex forms and additional parameters, but extensions of the present implicit potentials will become more tricky. For instance, the power law expressions of the Sutton–Chen potential [66] lead to the divergence of many integrals, starting with the atomic energy within

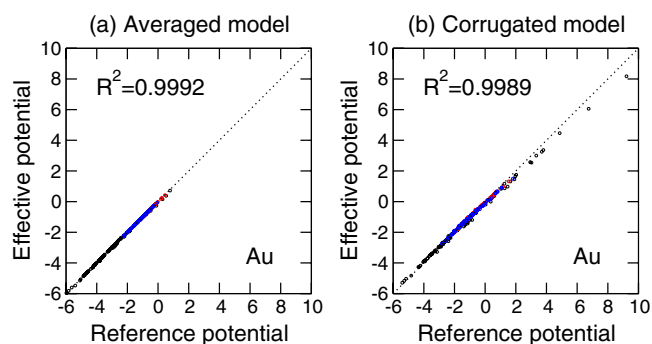


Figure 6. Correlation between the numerically exact interaction energy and the effective potential energy obtained for three adsorbates deposited on the (1 1 1) fcc gold surface. The various points represent random perturbations around the icosahedral structures of the 13- (red dots) and 55-atom (blue dots) clusters, or deformations of the two-dimensional 7-atom cluster (black dots). (a) Correlation between the uncorrugated potential \bar{V}_{eff} and the laterally averaged energy; (b) Correlation between the full potential V_{eff} and the exact interaction energy.

a monolayer (corresponding to the terms V_s^2 in the above derivation). Likewise, extensions to treat embedding functions other than the square root might be less straightforward in view of the important role played by the trick used to derive equation (2). However, due to the great flexibility offered by the generalized Morse functions, the present forms derived in this work from the underlying SMA potential could be used as a template for more sophisticated functional forms, on more rigorous grounds than using coordination-dependent parametrized forms. For instance, the embedding function acting on the effective electronic density n should still be present but incorporate an estimate of the contribution from the bulk substrate. The perturbation in the cohesive energy of the substrate, which numerically plays an equally important role as the perturbation of the electronic density, thus appears as the bottleneck for deriving such effective potentials.

6. Relaxation of nickel clusters on the (1 1 1) substrate

As a simple application of the effective model, we have investigated the relaxation of nickel clusters pre-formed in the gas phase and soft-landed onto the Ni(1 1 1) substrate. The deposition of metal clusters on surfaces has been identified as a possible method for thin film growth [67–69]. The shape obtained upon deposition is known to depend on a number of factors, including the collision energy [68] and the substrate temperature [70], as well as the cluster size itself [67–70]. It is generally understood that small clusters spontaneously wet the substrate due to the associated energetic gain, whereas large nanoparticles may sustain epitaxial contact without deforming too much [69].

Most simulations carried out so far have dealt with cubic nanoparticles, but nickel clusters produced in gas-phase experiments are more likely icosahedral or decahedral [71] until they reach a size sufficient to accommodate the less favorable (1 0 0) surfaces of the Wulff shapes. Icosahedral clusters exhibit (1 1 1) facets, also making them prone to contact epitaxy on the (1 1 1) substrate. The importance of substrate relaxation on the local deformation of those clusters has been evaluated by comparing the predictions of the effective potential with those of a fully atomistic minimization.

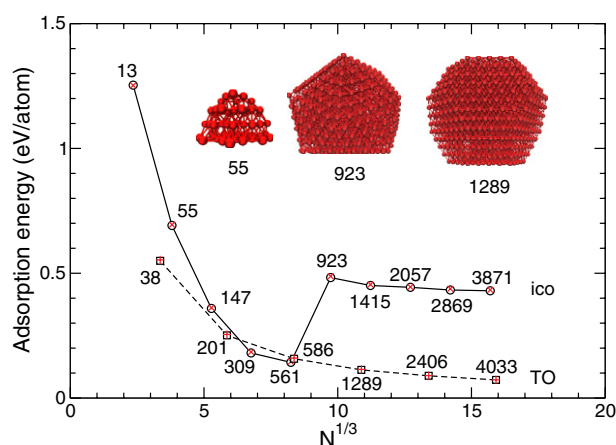


Figure 7. Adsorption energy of Ni_N nanoclusters on the $\text{Ni}(1\ 1\ 1)$ substrate, as obtained after local minimization at the fully atomistic level (black connected symbols) or using the effective model (red symbols) and as a function $N^{1/3}$. Icosahedral (ico, black circles and red star symbols) and truncated octahedral (TO, black squares and plus symbols) clusters are identified by their size, some of them being depicted as an inset.

To characterize the deposited clusters, we have considered the adsorption energy as the binding energy in the locally optimized structure relative to the energy at infinite separation and without deformation. For those initially spherical clusters, the magnitude of deformation upon contact can be simply evaluated from the principal momenta of inertia $A \geq B \geq C$ of the deposited structure, or equivalently from an asphericity index $\chi = 3(2A - B - C)/2(A + B + C)$.

All clusters were initially deposited in epitaxial contact with the $(1\ 1\ 1)$ surface, and then locally optimized. The variations of the minimized energy of the clusters is represented in figure 7 for icosahedral clusters in the range of 13–3871 atoms (up to 11 shells) and truncated octahedral clusters containing up to 4033 atoms (2 to 7 shells). From those minimizations, cubic clusters deposited on the $(1\ 1\ 1)$ substrate remain stable at 0 K and barely deform. The adsorption energy varies monotonically as the contact area increases. In contrast, small icosahedral clusters cannot accommodate the strain between the contact facet and the other inner parts, and they spontaneously deform to increase the contact epitaxial area. This effect is spectacular on the 55-atom cluster, which essentially loses its multilayer character. It is still apparent on larger clusters, and even in the 6-shell cluster Ni_{923} a settling down of the contact facet is clearly seen. In comparison, the truncated octahedral cluster of comparable size Ni_{1289} barely shows any deformation perpendicularly to the substrate. For these static results, the effective model necessarily overestimates the adsorption energy with respect to the fully atomistic model because it does not account for the local relaxation on contact. However, this discrepancy does not exceed 0.1%, and the model can be considered as reasonably accurate.

Next, short Monte Carlo simulations have been performed at 300 K to assess the finite temperature stability and possible further relaxation of those clusters under more realistic conditions. Those simulations were initialized from the previously determined locally stable minima. To compare the predictions of the effective model with the fully atomistic potential in those stochastic simulations, the same series of random numbers was used. We have represented in figure 8 the variations of the asphericity index χ obtained for selected clusters as the simulation proceeds, averaging the data over 10 Monte Carlo consecutive cycles to wash out some of the statistical noise. In general, the finite temperature contributes to further

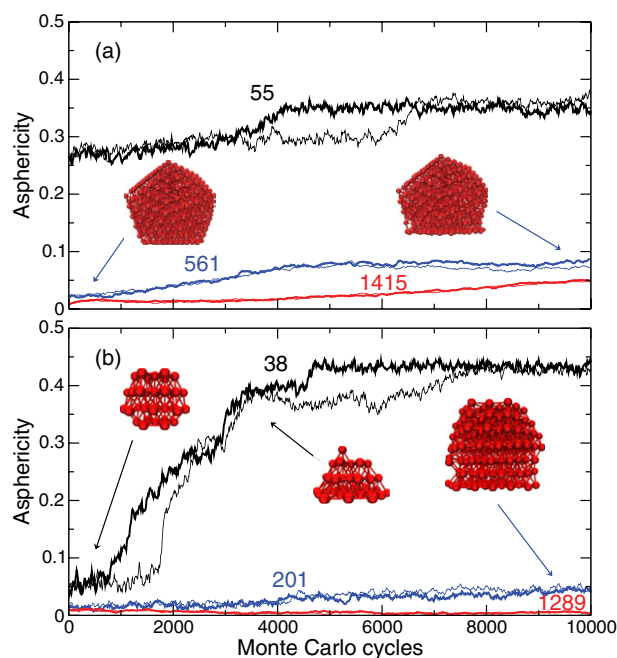


Figure 8. Global shape parameter as a function of Monte Carlo time during 300 K simulations of various nickel nanoclusters deposited on the Ni(1 1 1) substrate, as obtained from the fully atomistic model (thick lines) or from the effective model (thin lines). (a) Initially icosahedral clusters having 55, 561 or 1415 atoms; (b) Initially cubic clusters having 38, 201 or 1289 atoms. Some representative snapshots of the 561-, 38- and 201-atom clusters are also depicted.

deformations away from the spherical shape by allowing the clusters to overcome the local barriers and increase their epitaxial contact area. Such additional deformations are visible for Ni₅₅, although this cluster is already poorly spherical at 0 K. A stronger deformation is found for Ni₅₆₁, for which the strain experienced in the locally optimized structure is sufficient to shrink the layers above the contact facet in a non-reversible way. As thermal energy is poured into the system, the contact region becomes much less stable and undergoes further relaxation with the nanocluster flattening after about 5000 Monte Carlo cycles and subsequently stabilizing. In the 1415-atom icosahedral cluster, a similar evolution can be distinguished but taking place more slowly. After 10⁴ Monte Carlo cycles, none of the clusters has strictly remained in the initial local minimum it started from at the beginning of the trajectory. The resulting asphericity parameter probably becomes of more limited use in such larger nanoparticles.

Ni₃₈ spontaneously transforms to epitaxially wet the (1 1 1) substrate as the temperature is set to 300 K. However, as was the case for medium-sized icosahedral clusters, the larger Ni₂₀₁ nanocluster also experiences some deformation as the two layers at contact merge into a single broader one, the cluster looking as if it would soak into the substrate. Only the cubic Ni₁₂₈₉ cluster is able to sustain contact at 300 K without deforming significantly, at least under the short Monte Carlo trajectories that were simulated. Obviously, the kinetics of the transformation should be slower for large nanoparticles as it involves much more individual and collective motions.

At this low temperature, the effective model treating the substrate as rigid performs remarkably well with respect to the fully atomistic simulations. Although we do not expect it

to be suitable for studying the soft-landing process itself except at low collision energies, this agreement confirms the validity of the effective potential derived above, and supports its use beyond static studies.

7. Concluding remarks

The computational modeling of nanosized metallic adsorbates on metallic substrates is increasingly relevant in different areas of science and technology, and in such situations the role of the environment on the physical properties of the adsorbate simply cannot be neglected. The present work was aimed at building an analytic effective potential to describe metal-on-metal adsorption, based on a reference embedded-atom model potential in the second-moment approximation of the electronic density of states in tight-binding theory. The main contribution of this potential was derived at the mean-field level by integration of the substrate treated as an infinite set of equidistant monolayers. Such an integration relies on several exact steps and only one major approximation involving only four parameters. Corrugation was described more phenomenologically by adding symmetry-adapted correcting terms in the additive and many-body functions. By truncating the description of corrugation to the second order in the Fourier lateral expansion, 16 additional parameters are introduced and fitted together with the four parameters of the uncorrugated potential to reproduce the adsorption energies of a realistic training set of 300 random adsorbates.

Such effective potentials were extracted for adsorbates on (1 1 1) fcc surfaces of the same metal, taking the reference SMA potential from the work by Cleri and Rosato [61]. For those transition and noble metals, the general accuracy was found to be very good both for the averaged and corrugated versions of the potential. Obviously, the effective potentials we have derived are at least as approximate as the SMA model they are built from. In particular, the deficiencies inherent to the SMA model in general, such as the inability to describe bcc metals or the difficulties in reproducing surface reconstructions, and those specific to the Cleri–Rosato parametrization (only based on bulk properties) will of course convey to the present effective potentials. However, the mathematical approximations introduced here are not a mere academic exercise, as they are generally more robust than the physical approximations underlying the EAM models. Hence, we believe they should be valuable in providing a guiding framework for constructing generic semi-empirical effective potentials for adsorbates on crystalline substrates, to be parametrized not necessarily for semi-empirical models as well, but using independent, experimental or *ab initio* reference data.

Our simple application to the relaxation of nickel clusters soft-landed and in epitaxial contact with the Ni(1 1 1) substrate showed that icosahedra are locally stable only when they contain about 10^3 atoms or more, whereas all truncated octahedra are stable at 0 K. At room temperature, the smaller clusters flatten and wet the substrate but even large icosahedra remain globally stable except for some deformation at contact due to the higher stress they experience relative to cubic clusters.

Besides this straightforward application, future uses of the present effective model could be to provide simplified energy surfaces for global optimization and the search for low-energy structures, candidate minima being possibly refined using the complete reference potentials. Such a hierarchical optimization procedure is commonly employed in clusters physics [72], where analytical potentials guide the search for global minima to save most of the computational effort. At high temperatures, the approximation of a frozen substrate may become more questionable, but the present approach would remain of great interest for adsorbates that are less cohesive than their substrate.

It would also be useful to try to extend the present effort to more complex potentials having an angular contribution, such as modified EAM [58, 59] or even bond-order potentials [60, 73, 74]. Although it remains unclear how the integration could proceed with those angular terms, the analytic form offered by the effective potentials above could motivate practical approximations with dedicated angular corrections.

Acknowledgments

The project was funded by the Agence Nationale de La Recherche through the project ANR-10-BLAN-1019-04 NMGEM. We thank the regional Pôle Scientifique de Modélisation Numérique for generous allocation of computer resources.

Appendix: parameters for other noble and transition metals

Table 2 gives the set of optimized parameters for the nine metals other than gold studied by Cleri and Rosato [61].

Table 2. List of parameters of the effective potential for metallic adsorbates on (1 1 1) fcc surfaces, for a second-order Fourier expansion in lateral corrugation. The original SMA parameters from Cleri and Rosato [61] are also given for each metal.

Parameter	Unit	Ni	Cu	Rh	Pd	Ag	Ir	Pt	Al	Pb
p		16.999	10.960	18.450	10.867	10.928	16.980	10.612	8.612	9.576
q		1.189	2.278	1.867	3.742	3.139	2.691	4.004	2.516	3.648
ε	eV	0.0376	0.0855	0.0629	0.1746	0.1028	0.1156	0.2975	0.1221	0.0980
ξ	eV	1.070	1.224	1.660	1.718	1.178	2.289	2.695	1.316	0.914
r_0	Å	2.4911	2.5562	2.6891	2.7485	2.8885	2.7146	2.7747	2.8638	3.5009
a	10^{-2} Å	3.552	2.426	4.688	2.938	3.887	3.188	4.865	3.538	3.237
b	10^{-2} Å ²	1.632	2.382	3.037	0.434	0.001	1.584	0.228	0.043	0.052
A	$\times 10^{-4}$	8.43	4.68	2.68	7.74	3.95	6.90	19.29	1.84	2.82
B	$\times 10^{-2}$	3.23	9.90	17.3	21.8	20.4	16.2	63.1	10.49	13.8
C_1	10^{-2} eV	1.2	1.6	2.2	3.8	14.7	4.1	4.1	1.5	15.3
μ_1		17.49	12.74	18.90	11.50	9.38	17.30	12.34	10.56	8.95
D_1	10^{-2} eV	0.29	0.11	1.95	5.86	14.8	3.3	7.2	5.5	15.6
ν_1		1.27	2.65	6.51	3.63	8.26	7.50	4.44	7.11	8.40
C_2	10^{-3} eV	1.936	1.161	1.471	0.778	0.367	0.604	1.288	0.040	0.015
μ_2		6.87	3.31	22.10	9.62	13.96	24.84	9.71	13.68	18.61
D_2	10^{-3} eV	1.62	1.31	2.52	0.96	0.97	1.91	0.65	1.53	0.42
ν_2		2.50	0.86	4.68	2.67	3.11	0.70	0.19	1.84	1.73
W_1	10^{-2} eV	4.45	4.29	4.23	3.17	3.33	2.73	4.87	3.47	6.26
ω_1		6.87	14.33	18.02	14.10	11.20	22.16	4.95	5.97	11.68
I_1	10^{-3} Å ²	1.295	1.339	1.610	0.934	1.180	0.215	0.391	1.609	1.783
ρ_1		2.50	6.66	3.72	6.86	2.81	4.59	2.47	2.39	1.41
W_2	10^{-3} eV	7.45	7.41	6.15	5.23	7.02	6.72	5.58	9.64	7.15
ω_2		5.27	3.48	1.53	1.78	4.92	6.47	1.93	4.95	10.75
I_2	10^{-5} Å ²	7.38	6.47	4.81	11.53	11.07	1.18	2.36	4.56	3.32
ρ_2		4.94	1.61	6.46	4.48	4.79	8.43	3.89	0.30	0.53

References

- [1] Warshel A and Levitt M 1976 Theoretical studies of enzymic reactions—dielectric, electrostatic and steric stabilization of carbonium ion in reaction of lysozyme *J. Mol. Biol.* **103** 227–49
- [2] Tomasi J, Mennucci B and Cammi R 2005 Quantum mechanical continuum solvation models *Chem. Rev.* **105** 2999–3093
- [3] Steele W A 1973 The physical interaction of gases with crystalline solids. I. Gas-solid energies and properties of isolated adsorbed atoms *Surf. Sci.* **36** 317–52
- [4] Bretón J, González-Platas J and Girardet C 1994 Endohedral adsorption in graphitic nanotubes *J. Chem. Phys.* **101** 3334–40
- [5] Stan G and Cole M W 1998 Low coverage adsorption in cylindrical pores *Surf. Sci.* **395** 280–91
- [6] González B S and Hernández-Rojas J Bretón J and Gomez Llorente J M 2007 Global energy minima of $(\text{H}_2\text{O})_n$ clusters on graphite *J. Phys. Chem. C* **111** 14862–9
- [7] Morrow B H and Striolo A 2008 Platinum nanoparticles on carbonaceous materials: the effect of support geometry on nanoparticle mobility, morphology, and melting *Nanotechnology* **19** 195711 and references therein
- Neek-Amal M, Asgari R and Rahimi-Tabar M R 2009 The formation of atomic nanoclusters on graphene sheets *Nanotechnology* **20** 135602 and references therein.
- [8] Vervisch W, Mottet C and Goniakowski J 2002 Theoretical study of the atomic structure of Pd nanoclusters deposited on a MgO(1 0 0) surface *Phys. Rev. B* **65** 245411
- [9] Cortes-Huerto R, Goniakowski J and Noguera C 2013 An efficient many-body potential for the interaction of transition and noble metal nano-objects with an environment *J. Chem. Phys.* **138** 244706
- [10] Wang S C and Ehrlich G 1990 Structure, stability, and surface diffusion of clusters: Ir_x on Ir(1 1 1) *Surf. Sci.* **239** 301–32
- [11] Liu C-L and Adams J B 1992 Structure and diffusion of clusters on Ni surfaces *Surf. Sci.* **268** 73–86
- [12] Massobrio C and Blandin P 1993 Structure and dynamics of Ag clusters on Pt(111) *Phys. Rev. B* **47** 13687–94
- [13] Castellani N J and Legare P 1994 Homoepitaxy of small aggregates on Ni(1 1 1) and Pt(1 1 1): an extended Hückel study *Surf. Sci.* **320** 39–54
- [14] Breeman M, Barkema G T and Boerma D O 1995 Binding energies and stability of Cu-adatom clusters on Cu(1 0 0) and Cu(1 1 1) *Surf. Sci.* **323** 71–80
- [15] Chang C M, Wei, C M and Chen S P 1996 Modeling of Ir adatoms on Ir surfaces *Phys. Rev. B* **54** 17083–96
- [16] Wang S C and Ehrlich G 1997 Equilibrium shapes and energetics of iridium clusters on Ir(1 1 1) *Surf. Sci.* **391** 89–100
- [17] Longo R C, Rey C and Gallego L J 1999 Structure and melting of small Ni clusters on Ni surfaces *Surf. Sci.* **424** 311–21
- [18] Bogicevic A 1999 Metal-on-metal bonding and rebonding revisited *Phys. Rev. Lett.* **82** 5301–4
- [19] Zhuang J, Kojima T, Zhang W, Liu L, Zhao L and Li Y 2002 Structure of clusters on embedded-atom-method metal fcc (1 1 1) surfaces *Phys. Rev. B* **65** 045411
- [20] Zhuang J, Sun Z H, Zhang W H, Zhuang M, Ning X J, Liu L and Li Y F 2004 Structure and magic numbers of adatom clusters on metal fcc (0 0 1) surfaces *Phys. Rev. B* **69** 165421
- [21] Hristova E, Grigoryan V G and Springborg M 2009 Structures and stability of Ag clusters on Ag(1 1 1) and Ni(1 1 1) surfaces *Surf. Sci.* **603** 3339–45
- [22] Schmid M, Garhofer A, Redinger J, Wimmer F, Scheiber P and Varga P 2011 Unusual cluster shapes and directional bonding of an fcc metal: Pt/Pt(1 1 1) *Phys. Rev. Lett.* **107** 016102
- [23] Shiang K D and Tsong TT 1994 Molecular-dynamics study of self-diffusion: iridium dimers on iridium surfaces *Phys. Rev. B* **49** 7670–8
- [24] Ferrando R and Tréglia G 1995 Tight-binding molecular dynamics study of diffusion on Au and Ag(1 1 1) *Surf. Sci.* **331** 920–4
- [25] Bitar L, Serena P A, García-Mochales P, García N and Binh V T 1995 Mechanism for diffusion of nanostructures and mesoscopic objects on surfaces *Surf. Sci.* **339** 221–32

- [26] Shi Z-P, Zhang Z, Swan A K and Wendelken J F 1996 Dimer shearing as a novel mechanism for cluster diffusion and dissociation on metal (1 0 0) surfaces *Phys. Rev. Lett.* **76** 4927–30
- [27] Wang S C and Ehrlich G 1997 Diffusion of large surface clusters: direct observations on Ir(1 1 1) *Phys. Rev. Lett.* **79** 4234–7
- [28] Deltour P, Barrat J-L and Jensen P 1997 Fast diffusion of a Lennard-Jones cluster on a crystalline surface *Phys. Rev. Lett.* **78** 4597–600
- [29] Bogicevic A, Hyldgaard P, Wahnström G and Lundqvist B I 1998 Al dimer dynamics on Al(1 1 1) *Phys. Rev. Lett.* **81** 172–5
- [30] Linderöth T R, Horch S, Petersen L, Helveg S, Lægsgaard E, Stensgaard I and Besenbacher F 1999 Novel mechanism for diffusion of one-dimensional clusters: Pt/Pt(1 1 0)-(1x2) *Phys. Rev. Lett.* **82** 1494–7
- [31] Boisvert G and Lewis L J 1999 Diffusion of Pt dimers on Pt(1 1 1) *Phys. Rev. B* **59** 9846–9
- [32] Kürpick U, Fricke B and Ehrlich G 2000 Diffusion mechanisms of compact surface clusters: Ir₇ on Ir(1 1 1) *Surf. Sci. Lett.* **470** L45–51
- [33] Kürpick U 2002 Effect of adsorbate interactions on adatom self-diffusion on Cu(1 1 1) and Ni(1 1 1) surfaces *Phys. Rev. B* **66** 165431
- [34] Zhuang J, Liu Q W, Zhuang M, Liu L, Zhao L and Li Y F 2003 Exchange rotation mechanism for dimer diffusion on metal fcc (0 0 1) surfaces *Phys. Rev. B* **68** 113401
- [35] Goyhenex C 2006 Adatom and dimer migration in heteroepitaxy: Co/Pt(1 1 1) *Surf. Sci.* **600** 15–22
- [36] Morgenstern K, Braun K F and Rieder K H 2004 Direct imaging of Cu dimer formation, motion, and interaction with Cu atoms on Ag(1 1 1) *Phys. Rev. Lett.* **93** 056102
- [37] Morgenstern K and Rieder K H 2005 Long-range interaction of copper adatoms and copper dimers on Ag(1 1 1) *New. J. Phys.* **7** 139
- [38] Yang J Y, Hu W Y, Tang J F and Xu M C 2008 Long-time scale molecular dynamics study of diffusion dynamics of small Cu clusters on Cu(1 1 1) surface *J. Phys. Chem. C* **112** 2074–8
- [39] Liu F S, W. Y. Hu, Deng H Q, Luo W H, Xiao S F and Yang J Y 2009 Self-diffusion dynamic behavior of atomic clusters on Re(0 0 1) surface *Appl. Surf. Sci.* **21** 8883–9
- [40] Liu F, Hu W Y, Deng H Q, He R S, Yang X Y, Luo W H, Lu K L and Deng L 2010 Dynamics diffusion behaviors of Pd small clusters on a Pd(1 1 1) surface *Modelling Simul. Mater. Sci. Eng* **18** 045010
- [41] Signor A W and Weaver J H 2011 Preferential nucleation and high mobility of linear Cu trimers on Ag(1 1 1) *Phys. Rev. B* **84** 165441
- [42] Karim A, Kara A, Trushin O and Rahman T S 2011 The crossover from collective motion to periphery diffusion for two-dimensional adatom-islands on Cu(1 1 1) *J. Phys.: Condens. Matter* **23** 462201
- [43] Shah S I, Nandipati G, Kara A and Rahman T S 2013 Self-diffusion of small Ni clusters on the Ni(1 1 1) surface: a self-learning kinetic Monte Carlo study *Phys. Rev. B* **88** 035414
- [44] Kellogg G L and Feibelman P J 1990 Surface self-diffusion on Pt(0 0 1) by an atomic exchange mechanism *Phys. Rev. Lett.* **64** 3143–6
- [45] Chen C and Tsong T T 1990 Displacement distribution and atomic jump direction in diffusion of Ir atoms on the Ir(0 0 1) surface *Phys. Rev. Lett.* **64** 3147–50
- [46] Shiang K-D, Wei C M and Tsong T T 1994 A molecular dynamics study of self-diffusion on metal surfaces *Surf. Sci.* **301** 136–50
- [47] Zhuang J and Liu L 1998 Exchange mechanism for adatom diffusion on metal fcc(1 0 0) surfaces *Phys. Rev. B* **58** 1173–6
- [48] Fordell T, Salo P and Alatalo M 2002 Self-diffusion on fcc(1 0 0) metal surfaces: comparison of different approximations *Phys. Rev. B* **65** 233408
- [49] Antezak G and Ehrlich G 2007 Jump processes in surface diffusion *Surf. Sci. Rep.* **62** 39–61
- [50] Yildirim H, Kara A and Rahman T S 2007 Origin of quasi-constant pre-exponential factors for adatom diffusion on Cu and Ag surfaces *Phys. Rev. B* **76** 165421
- [51] Wen Y-N, Zhang J-M and Xu K-W 2009 Diffusion of single adatom Cu on Cu(0 0 1) and (1 1 0) surfaces *Appl. Surf. Sci.* **256** 1521–5

- [52] Hayat S S, Alcantara Ortigoza M, Choudhry M A and Rahman T S 2010 Diffusion of the Cu monomer and dimer on Ag(1 1 1): molecular dynamics simulations and density functional theory calculations *Phys. Rev. B* **82** 085405
- [53] Fijak R, Jurczynszyn L and Antczak G 2011 Movement of a tungsten adatom on the W(1 1 2) surface *Surf. Sci.* **605** 282–8
- [54] Chen Z and Ghoniem N 2013 Biaxial strain on adatom surface diffusion on tungsten from first principles *Phys. Rev. B* **88** 035415
- [55] Cyrot-Lackmann F 1968 Sur le calcul de la cohésion et de la tension superficielle des métaux de transition par une méthode de liaisons fortes *J. Phys. Chem. Solids* **29** 1235–43
- [56] Ducastelle F 1970 Modules élastiques des métaux de transition *J. Phys. (Paris)* **31** 1055–62
- [57] Daw M S and Baskes M I 1983 Semiempirical, quantum mechanical calculation of hydrogen embrittlement in metals *Phys. Rev. Lett.* **50** 1285–8
- [58] Baskes M I 1987 Application of the embedded-atom method fo covalent materials: a semiempirical potential for silicon *Phys. Rev. Lett.* **59** 2666–9
- [59] Baskes M I, Nelson J S and Wright A F 1989 Semiempirical modified embedded-atom potentials for silicon and germanium *Phys. Rev. B* **40** 6085–100
- [60] Brenner D W 1989 Relationship between the embedded-atom method and Tersoff potentials *Phys. Rev. Lett.* **63** 1022
- [61] Cleri F and Rosato V 1993 Tight-binding potentials for transition metals and alloys *Phys. Rev. B* **48** 22–33
- [62] Gupta R P 1981 Lattice relaxation at a metal surface *Phys. Rev. B* **23** 6265–70
- [63] Bocchetti V and Diep H T 2013 Monte Carlo simulation of melting and lattice relaxation of the (1 1 1) surface of silver *Surf. Sci.* **614** 46–52
- [64] Pu Q, Leng Y, Tsetseris L, Park H S and Pantelides S T and Cummings P T 2007 Molecular dynamics simulations of stretched gold nanowires: The relative utility of different semiempirical potentials *J. Chem. Phys.* **126** 144707
- [65] Ferrando R, Fortunelli A and Johnston R L 2008 Searching for the optimum structures of alloy nanoclusters *Phys. Chem. Chem. Phys.* **10** 640–9
- [66] Sutton A P and Chen J 1990 Long-range Finnis–Sinclair potentials *Phil. Mag. Lett.* **61** 139–46
- [67] Yeadon M, Yang J C, Ghaly M, Averbach R S and Murray Gibson J 1999 Novel interactions of supported clusters: contact epitaxy *Mater. Sci. Eng. B* **67** 76–9
- [68] Bardotti L, Prével B, Mélinon P, Perez A, Hou Q and Hou M 2000 Deposition of Au_N clusters on Au(1 1 1) surfaces: II. Experimental results and comparison with simulations *Phys. Rev. B* **62** 2835–42
- [69] Järvi T T, Kuronen A, Meinander K, Nordlund K and Albe K 2007 Contact epitaxy by deposition of Cu, Ag, Au, Pt, and Ni nanoclusters on (1 0 0) substrates: Size limits and mechanisms *Phys. Rev. B* **75** 115422
- [70] Lee S-C, Yu B D, Kim D-Y and Hwang N M 2002 Effects of cluster size and substrate temperature on the homoepitaxial deposition of Au clusters *J. Cryst. Growth* **242** 463–70
- [71] Cleveland C L and Landman U 1991 The energetics and structure of nickel clusters: size dependence *J. Chem. Phys.* **94** 7376–96
- [72] Hartke B 1993 Global geometry optimization of clusters using genetic algorithms *J. Phys. Chem.* **97** 9973–6
- [73] Abell G C 1985 Empirical chemical pseudopotential theory of molecular and metallic bonding *Phys. Rev. B* **31** 6184–96
- [74] Tersoff J 1986 New empirical model for the structural properties of silicon *Phys. Rev. Lett.* **56** 632–5